Int J CARS (2015) 10:497–508
DOI 10.1007/s11548-014-1116-7

ORIGINAL ARTICLE

Development of a biomechanical guidance system for periacetabular osteotomy

Ryan J. Murphy · Robert S. Armiger · Jyri Lepistö · Simon C. Mears · Russell H. Taylor · Mehran Armand

Received: 16 May 2014 / Accepted: 2 September 2014 / Published online: 19 September 2014

Abstract
Purpose This paper presents and validates a computer-navigated system for performing periacetabular osteotomy (PAO) to treat developmental dysplasia of the hip. The main motivation of the biomechanical guidance system (BGS) is to plan and track the osteotomy fragment in real time during PAO while simplifying the procedure for less-experienced surgeons. The BGS aims at developing a platform for comparing biomechanical states of the joint with the current gold standard geometric assessment of anatomical angles. The purpose of this study was to (1) determine the accuracy with which the BGS tracks the hip joint through repositioning and (2) identify improvements to the workflow.
Methods Nineteen cadaveric validation studies quantified system accuracy, verified system application, and helped to refine surgical protocol. In two surgeries, navigation and registration accuracy were computed by affixing fiducials to two cadavers prior to surgery. All scenarios compared anatomical angle measurements and joint positioning as measured intraoperatively to postoperatively.
Results In the two cases with fiducials, computed fragment transformations deviated from measured fiducial transformations by 1.4 and 1.8 mm in translation and 1.0° and 2.2° in rotation, respectively. The additional seventeen surgeries showed strong agreement between intraoperative and postoperative anatomical angles, helped to refine the surgical protocol, and demonstrated system robustness.
Conclusion Estimated accuracy with BGS appeared acceptable for future surgical applications. Several major system requirements were identified and addressed, improving the BGS and making it feasible for clinical studies.

Keywords Periacetabular osteotomy · Developmental dysplasia · Computer-assisted surgery · Orthopedics

R. J. Murphy (✉) · R. S. Armiger · M. Armand
Research and Exploratory Development Department, Johns Hopkins University Applied Physics Laboratory, 11100 Johns Hopkins Rd, 21-S100, Laurel, MD 20723, USA
e-mail: Ryan.Murphy@jhuapl.edu

R. S. Armiger
e-mail: Robert.Armiger@jhuapl.edu

M. Armand
e-mail: Mehran.Armand@jhuapl.edu

R. J. Murphy · M. Armand
Department of Mechanical Engineering, Johns Hopkins University, Baltimore, MD, USA

J. Lepistö
Orton Orthopaedic Hospital, Helsinki, Finland
e-mail: jyri.lepisto@fimnet.fi

S. C. Mears
Department of Orthopedic Surgery, Baylor Regional Medical Center at Plano, Plano, TX, USA
e-mail: simon_mears@hotmail.com

R. H. Taylor
Department of Computer Science, Johns Hopkins University, Baltimore, MD, USA
e-mail: rht@jhu.edu

Introduction

The Bernese (Ganz) periacetabular osteotomy (PAO) [1] is a technically challenging procedure [2] used as a common treatment option for patients suffering from developmental dysplasia of the hip (DDH). For those suffering from DDH, the acetabulum is reduced in size compared to a normal hip, creating reduced coverage of the femoral head, which leads to osteoarthritis and significant pain for the patient [3]. During the PAO procedure, a series of multiple surgical cuts around the hip joint free the acetabulum from the pelvis [1]. These

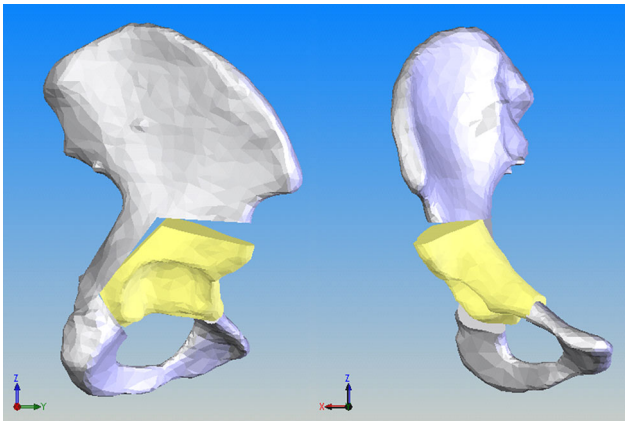

Fig. 1 Example cuts for a periacetabular osteotomy. Note the cut does not disturb the integrity of the posterior column of the pelvis or interfere with the hip joint

cuts must be made with limited line of sight and cannot fracture the posterior column of the pelvis or damage the hip joint (Fig. 1). After releasing the acetabular fragment, the surgeon repositions the hip joint and fixes the fragment with bone screws. Periacetabular osteotomy seeks to reposition the hip joint to a more "normal" geometric configuration, thereby increasing coverage of the femoral head to that observed in normal hips and reducing joint pressure [1,2].

Standard PAO feedback regarding joint repositioning and tool placement is limited to visualization from planar, C-arm X-ray images, and a surgeon's experience with tactile feedback from pelvic structure. Accurately achieving the planned/correct 3D joint positioning of the fragment in the intraoperative environment is especially difficult [4]. Moreover, studies suggest that the joint repositioning should be checked intraoperatively to improve survivorship [5,6]. Tool navigation systems for PAO assist surgeons in making difficult cuts which they cannot perform with direct line of sight [7,8]. However, tool tracking only addresses the technical challenge of surgically releasing the acetabulum and does not provide biomechanical or 3D geometrical feedback regarding joint repositioning. Real-time feedback of the joint repositioning and simulated joint contact pressures has the potential to provide the surgeon necessary information to select and achieve optimal joint repositioning [6,9–12].

Preoperative planning to achieve an optimal joint repositioning is an important component of PAO; however, preoperative information is limited and may not fully characterize the ability to execute the plan. Moreover, intraoperatively, the surgeon must assess certain factors such as quality and stability of fixation, requiring active decision-making to evaluate trade-offs in real time. In most cases, the surgeon will modify the preoperative plan based on intraoperative observations. Therefore, a system that updates the plan immediately and interactively with information regarding joint repositioning and biomechanical factors provides the most available up-to-date information.

This paper presents a system overview of the biomechanical guidance system (BGS). To our knowledge, the BGS [13,14] is the first system that provides real-time intraoperative guidance related to both geometric (radiographic angles) and biomechanical parameters, and incorporates these details into patient-specific plan updates for PAO. This study also addresses the following research questions: (1) What is the accuracy of the BGS system in tracking the acetabular fragment? and (2) How can we improve system feasibility in surgical practice?

Materials and methods

BGS description

The BGS consists of a navigation camera (Polaris, NDI, Inc., Waterloo, CA), an instrumented spherical-tip pointing probe tracked using a rigidly fixed reference tool, a patient-mounted reference tool, and a software package that links the navigation camera and computes the biomechanical parameters and radiological measurements (Fig. 2). The BGS provides a preoperative planning module, an intraoperative registration and tracking module, and tools for intra- and postoperative evaluation (Fig. 3). The planning tools allow the surgeon to load patient-specific anatomy of the dysplastic hip, run optimization algorithms to automatically develop a target repositioning plan to minimize contact pressure, manually adjust the plan, and compute predicted contact pressures for simulated activities (Fig. 2). The intraoperative tracking module registers the patient to the computer model, updates the fragmented acetabular position based on the execution of the surgery, and provides visual feedback to the surgeon (Fig. 2). Tracking the repositioned acetabulum allows the surgeon to assess the location of the acetabular fragment by looking at acetabular orientation measurements, predicted contact pressures, and range of motion. Postoperative tools assess the BGS and compare the measured orientation of the acetabulum intraoperatively versus the joint repositioning from postoperative CT/MRI data.

Three-dimensional models of the pelvis and hip joint are computed from segmented preoperative CT scans including the superior aspect of the iliac wings to the inferior aspect of the pubic symphysis. The segmentation is initialized through an automated threshold-based segmentation of the bony anatomy. Manual refinement separates the pelvis and femur, and improves the segmentation. Commercial image processing software was used for the segmentation (Amira, Visualization Sciences Group, Burlington, MA). The BGS uses meshed surface models generated from the segmented bones for visualization of the patient-specific anatomy and plan-

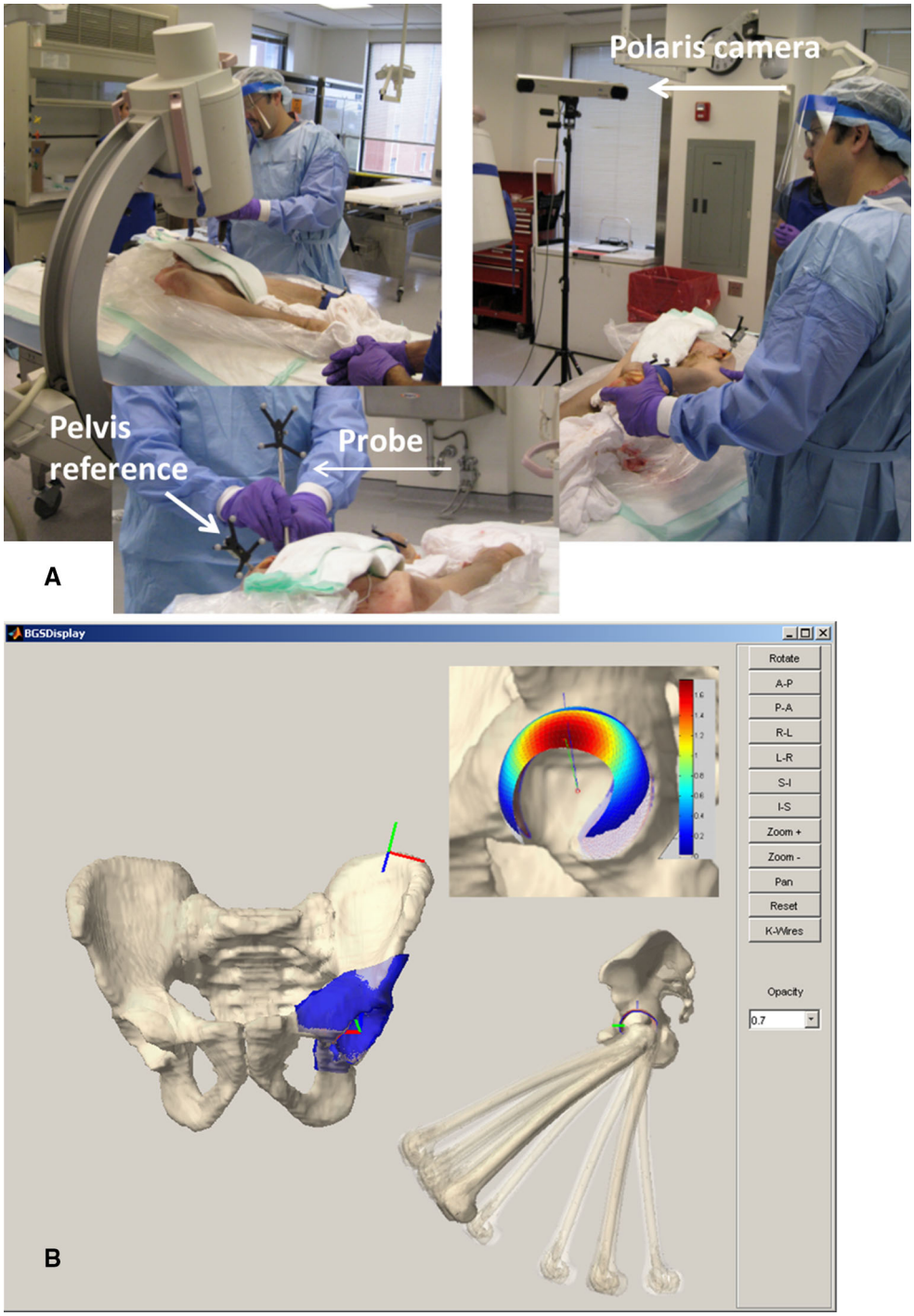

Fig. 2 Physical setup (**a**) and user interface (**b**) for the BGS system. The surgical setup highlights the minimal hardware required for operation: a Polaris camera, the digitizing probe, and the reference body attached to the pelvis. The user interface provides a real-time display of the acetabular fragment repositioning, areas of peak contact pressure estimated within the joint articular surface, and the range-of-motion of the femur recorded intraoperatively

ning the location of the osteotomies. Users select the medial and lateral walls of the acetabulum on reformatted oblique CT image slices extending radially from the center of the femoral head to define the articular surface model [15]. This model of the load bearing surface assumes correspondence between the subchondral bone of the acetabulum visible in the CT scan [15] and is input into a biomechanical model of the hip. The biomechanical model uses linear [10,16,17] or non-linear [18] discrete element analysis (DEA), which has been validated for various joints [19–22] to estimate contact

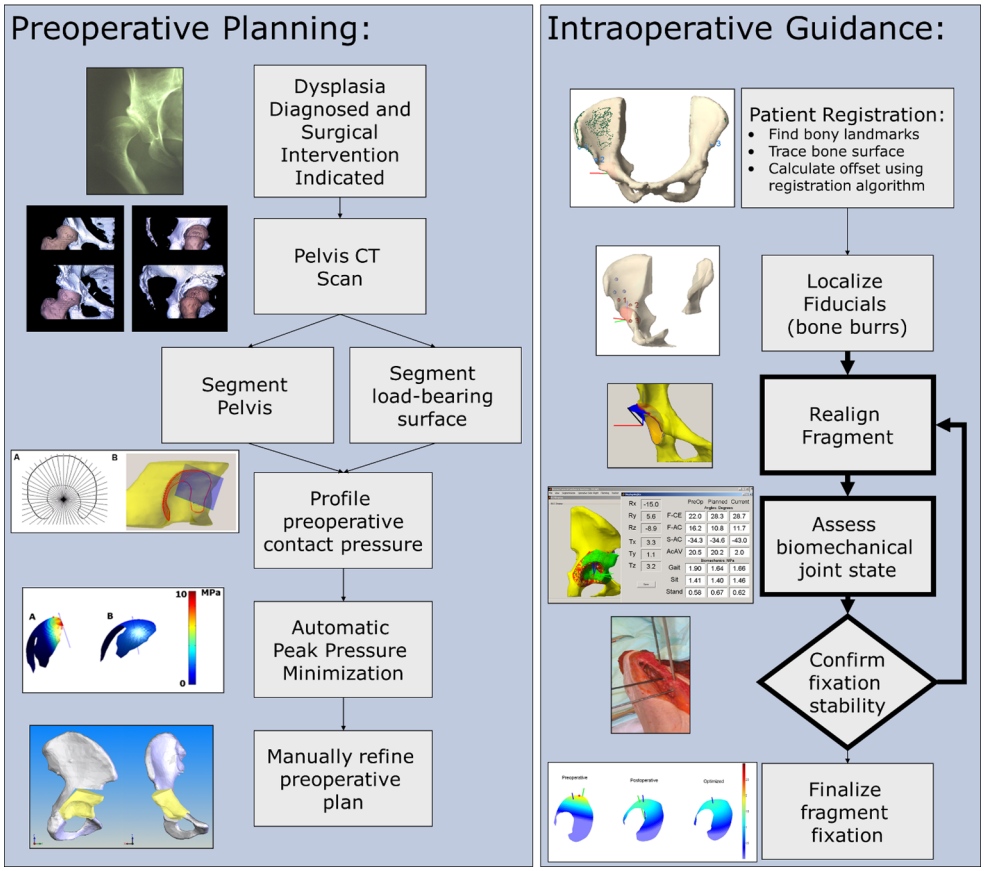

Fig. 3 Workflow for the BGS system

pressures. Briefly, this approach models the cartilage region as compressive springs and assumes no deformation of the bone in response to load. The nonlinear approach models cartilage behavior with greater detail and with more accuracy than classical, linear DEA; however, linear DEA offers reasonable approximations for cartilage strains not exceeding 30 % [18]. As such, linear DEA is the default choice in the BGS.

The BGS also performs geometric characterization of the acetabulum using radiographic angles measured through CT reformats and X-ray projections (Fig. 4). On the CT reformats, the angles of interest include the center edge (F-CE) [23,24] and acetabular inclination (F-AC) [24] in the frontal plane, the superior-anterior coverage (S-AC) [24,25] in the sagittal plane and the acetabular anteversion (AcetAV) [26,27] in the transverse plane. The F-CE angle measures lateral coverage; the F-AC angle indicates obliqueness of the acetabular roof; the S-AC angle defines orientation of the acetabular cup in the sagittal plane; the AcetAV measures anteversion. These characterizations are based on the preference of a collaborating surgeon (the co-author of this paper who has completed more than 350 PAO cases) and can be modified to fit individual surgeon preferences. A previously validated technique [15] automatically measures CT reformat angles using the segmented acetabulum. The BGS evaluates X-ray projection angles (CE and AC) by simulating an AP projection of the acetabular contour. From the projected contour, we extract the most lateral aspect of the contour and the medial aspect of the sourcil. These points define the radiographic CE [28] and AC [29] angles. Using two radiographic approaches (CT reformats and X-ray projection), the BGS provides complete information that translates between preoperative scan data and intraoperative projection C-arm data.

A calibrated pointing tool 200 mm in length with a spherical tip (radius of 1.1 mm) curving 15° digitizes points throughout the surgery. A spherical-tip probe glides more easily across the surface of the bone (as compared to a pointed probe) without risk of damaging the periosteum of the bone and settles repeatedly in bone-burr fiducials created as part of the navigation procedure. The curved tip allows easier access to the lateral aspect of the iliac wing.

The surgeon mounts a reference rigid body to either the contralateral or ipsilateral iliac crest using a 20×4 mm bone pin (Stryker, Kalamazoo, MI, USA). Applying the reference tool to the contralateral side maintains full accessibility of the

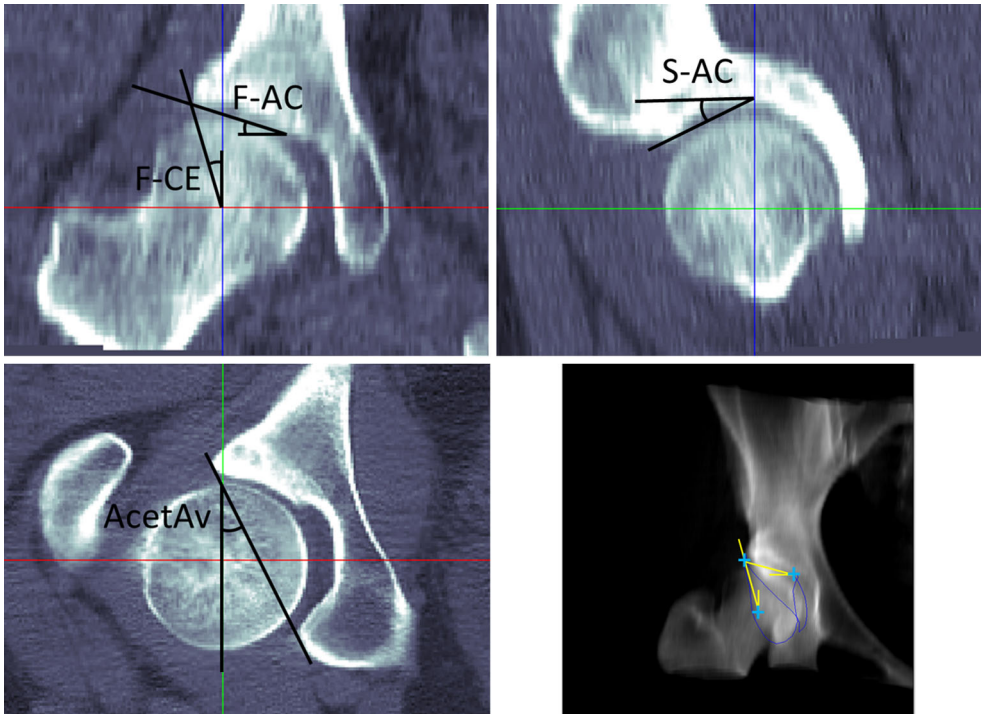

Fig. 4 Anatomical angles identified through CT reformats in the (*top left*) coronal, (*top right*) sagittal, (*bottom left*) transverse, and (*bottom right*) X-ray images. In the simulated X-ray image (*bottom right*), the acetabular rim is shown by the *blue line*; the *cyan* "*plus*" marks represent the locations defining the following points used in making measurements: from *left-to-right*, the most lateral aspect of the acetabular rim, the center of the femoral head, and the most medial aspect of the sourcil

operational exposure, which would result in a small (approximately 10–20 mm) incision on the non-operative side; however, this approach reduces the accuracy of the patient registration. With a detachable reference geometry, the ipsilateral approach is preferred to improve accuracy and maintain accessibility of the exposure. The BGS aligns the computer model to the patient using a two-stage registration process. First, a coarse registration is performed by selecting anatomical landmarks from both the patient's pelvis (using the navigated pointing probe) and the pelvis model (using a computer mouse). Locations of these registration landmarks are the anterior superior iliac spine (ASIS), the anterior inferior iliac spine (AIIS), and the ASIS on the contralateral side above the skin (Fig. 5). Surface points collected from accessible bony regions (Fig. 5) using the navigated pointing probe improve the registration through either an iterative closest points (ICP) [30] or unscented Kalman filter (UKF) [31] technique. While ICP is a widely used registration technique, UKF provides more stability and increases the chances of convergence when the error in the coarse initial registration is high [31].

After registration, the surgeon creates and digitizes four burrs on the expected fragment (Fig. 5) to localize the fragment throughout the surgery. Using bone burrs rather than mounting additional reference bodies has the advantage of not obstructing, occluding, or impeding the mobilization of the acetabular fragment. The radius of the burrs (1.0 mm) is slightly smaller than the probe's spherical tip, preventing the tip from penetrating through the cortical bone into the soft cancellous bone, thereby ensuring repeatable digitization.

Once the acetabulum is mobilized, the surgeon repositions the joint. The acetabulum is temporarily fixed and localized by digitizing the four fragment bone-burr locations. The BGS then instantaneously updates the virtual display, biomechanical contact pressure estimates, acetabular orientation measurements, geometric characterization, and current position compared to the planned location. The surgeon weighs these factors with those observed intraoperatively (e.g., quality of fixation, stability, and vascular supply) and determines whether the current position is acceptable or further adjustment is required. After successful repositioning, the fragment is fixed, the navigation tools removed, and the exposure closed.

BGS testing and validation studies

A total of nineteen cadaver tests were performed, separated into two cases: (1) Two instrumented cadaveric studies on separate, non-osteoporotic specimens (white female, age 79 and 64) with normal hips investigated the fragment tracking accuracy of the BGS. These validation tests provided

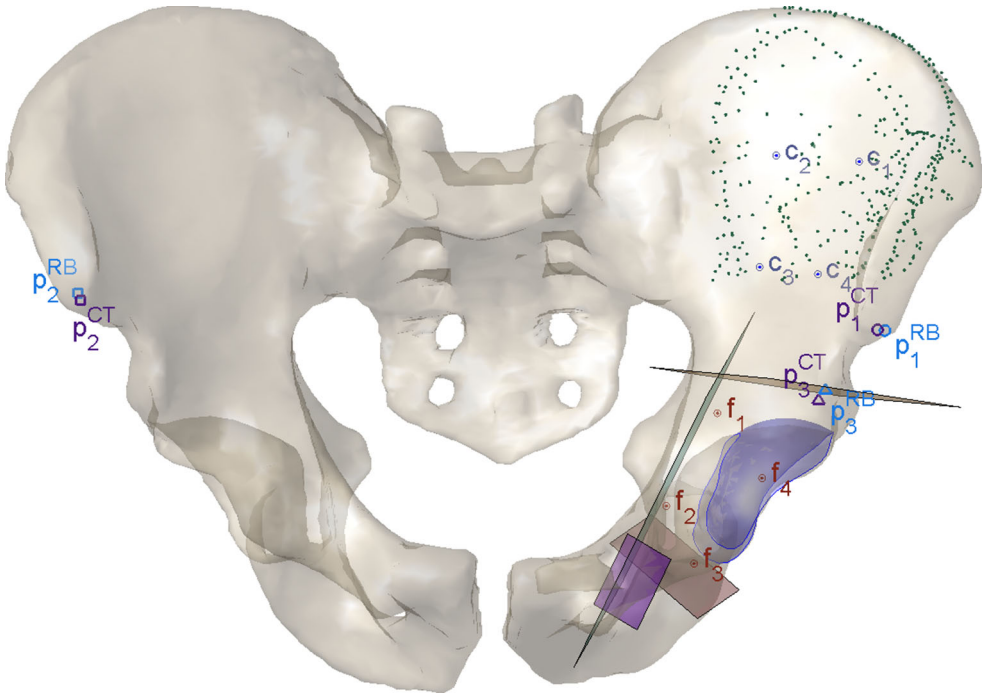

Fig. 5 Example pelvis display during surgery from cadaveric data. The colored planes represent the planned osteotomy lines; c_i are the confidence points; f_i are the fragment points; p_i^{RB} are the points digitized by the tracker and transformed into the CT frame; p_i^{CT} are the anatomical landmarks; the *green dots* are the collected surface points. The acetabular rim and articular surface are highlighted in *blue*

the highest accuracy characterization of the predicted versus actual joint repositioning. (2) Seventeen additional studies on twelve specimens using a clinically relevant approach (a) demonstrated clinical feasibility of the BGS; (b) evaluated the BGS as a system; and (c) verified system performance when major modifications to, or additions of, software modules or procedures occurred (e.g., addition of modules for the measurement of the hip range of motion). The non-osteoporotic, non-dysplastic specimens were obtained from the Maryland State Anatomy Board. Non-dysplastic (i.e., normal) specimens were sufficient as the objective was to test the system workflow and accuracy.

Preoperative data preparation followed the procedures described above. Specifically, CT scans were acquired between 0.5 and 2.0 mm slice thickness (resampled to 1.0 mm) with a pixel resolution between 0.65 and 0.95 mm. The scan extents included the superior aspect of the iliac wings to the inferior aspect of the pubic symphysis. These scans were segmented to define the pelvis and acetabular surface. The intraoperative workflow followed the procedures described in the "BGS description" section. For all specimens, linear DEA was used to compute biomechanics. The fragment repositioning was continually visualized throughout the surgery. During partial fixation, the surgeon was presented with the current anatomical angles and biomechanics.

In the two cadaveric cases testing navigation accuracy, fiducials (screws) were inserted preoperatively into the fixed portion of the pelvis and the acetabular fragment (Fig. 6). These fiducials were segmented from preoperative and postoperative CT scans to define the "ground-truth" fragment transformation. In these surgeries, bone burrs were still created on the fragment and the screws were not used for navigation. For instrumented cadaver trial #1, an arbitrary transformation was applied to the acetabular fragment; for instrumented cadaver trial #2, a more typical acetabular repositioning was applied to increase lateral coverage (Y axis) while minimizing out of plane rotations. Each of these surgeries had the pelvic reference attached on the contralateral iliac crest. In these surgeries, we compared the ICP and UKF patient registration methods as $F_{\mathrm{err}} = (F_{\mathrm{ICP}})^{-1} F_{\mathrm{UKF}}$ where F_{ICP} is the ICP-based registration and F_{UKF} is the UKF-based registration.

The studies on the remaining seventeen cadavers with intact joints focused on procedural refinement, system robustness, and software stability. This set of seventeen cadavers has no ground-truth to compare the fragment repositioning computed through the BGS system. The first eight cadaver surgeries were performed prior to the instrumented cadaver trials to refine the system and introduce the surgeon to the workflow. Intraoperative registration was performed using the UKF algorithm for the first nine specimens, and ICP for the remaining eight.

Postoperatively, we assessed the repositioning of the joint and compared this with the intraoperative measurement. The

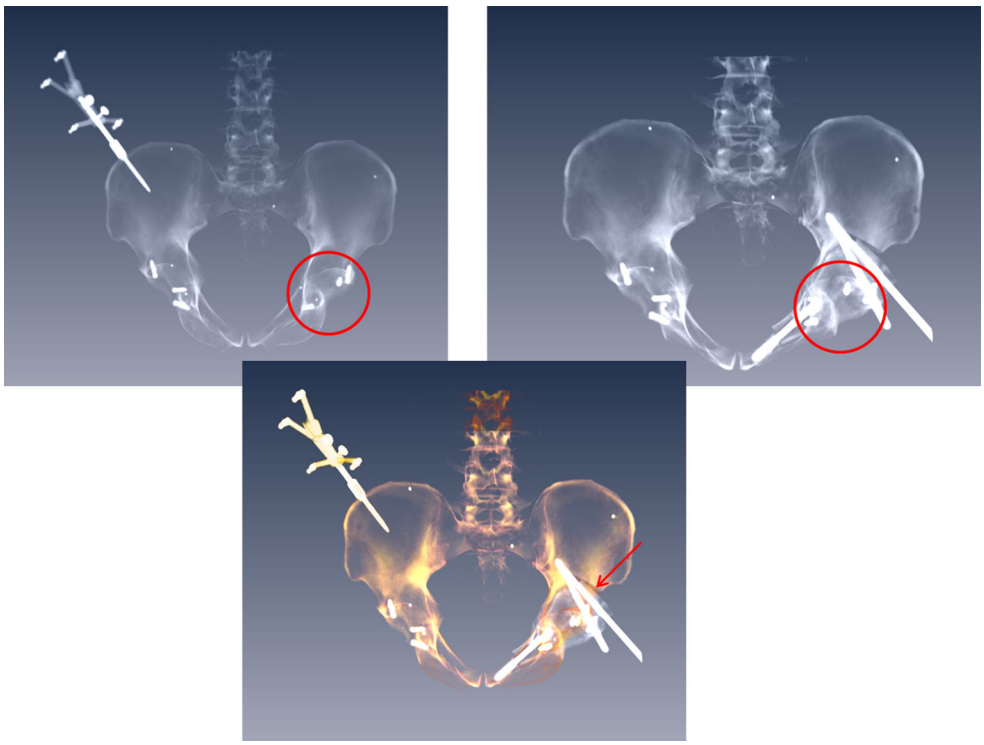

Fig. 6 Simulated X-ray images of a pelvis with fiducials. The *red circles* on the *top left* (preoperative) and *top right* (postoperative) images indicate the position of fiducial screws attached to the fragment. The *bottom image* is an overlay of the pre- and postoperative images with the preoperative image in the *orange* hue. The *red arrow* indicates the superior osteotomy cut

fixed portion of the pelvis from a postoperative CT scan is rigidly registered to the preoperative scan using normalized image cross-correlation (Amira, Visage Imaging Inc., San Diego, CA). This approach uses an extensive direction optimizer for initial registration followed by a quasi-Newton approach at the finer levels. Once registered, the acetabular contour is extracted [15] to directly compute the postoperative anatomical angles and biomechanics. Additionally, the segmented postoperative contour is registered to the preoperative contour using a point-based ICP technique to provide a second measure of the relative transformation of the fragment as a result of the osteotomy, the "postoperative contour registration (PCR)". We compute anatomical angles and biomechanics by applying the transformation to the preoperative acetabular contour and can compare these results to those measured intraoperatively. A one-way ANOVA was computed for the change in anatomical angles from the preoperative values as measured by the BGS, PCR, and postoperative methods.

Results

The average transformation applied to the acetabular fragment across all nineteen surgeries was 8.3 ± 5.1 mm and $17.5° \pm 9.6°$. The average difference in anatomical angles measured intraoperatively and preoperative were $6.2° \pm 9.8°$ for F-CE, $-4.7° \pm 9.6°$ for F-AC, $11.3° \pm 7.6°$ for CE, and $-9.1° \pm 7.1°$ for AC. The average intraoperative patient registration error was 0.7 ± 0.4 mm. Throughout the trials, the surgeons gained more experience and became comfortable with the system.

The instrumented cadaver trials showed the BGS and PCR transformation measurements do not have large differences compared to the ground-truth fiducial measurements (Table 1). The BGS measured fragment transformation did not deviate more than 2.2 mm and 1.8° compared to the ground truth; the PCR computation did not deviate more than 1.8 mm and 3.9°. The automated angle computation for the CT-based angles (F-CE, F-AC, S-AC, AcetAv) and the radiographic projections (CE, AC) exhibited similar consistency to the fragment tracking errors (Table 2). In both instrumented cadaver tests, the computation of the geometric acetabular angles from the direct postoperative segmentation had the largest magnitude error discrepancy with the fiducial-based measurements: $2.7° \pm 2.4°$ compared to $1.1° \pm 0.7°$ and $1.3° \pm 0.9°$ for the BGS intraoperative and PCR approach, respectively (Table 2). The differences between ICP and UKF were 0.8 mm and 0.4° for cadaver #1, and 1.9 mm and 0.3° for cadaver #2.

The seventeen additional cadaver studies showed that the BGS intraoperative anatomical angle measurements bet-

Table 1 Measured fragment transformations through varying approaches

	Cup rotation (Rxyz, deg)	Cup translation (mm)	Rotation error (deg)	Translation error (mm)
Trial 1 (*left hip*)				
Gold standard	[−11.8, −13.7, 9.7]	[3.6, 6.6, −1.1]	0	0
BGS	[−10.5, −13.3, 9.0]	[3.8, 6.1, −0.2]	1.4	1.0
PCR	[−8.2, −14.3, 10.4]	[3.3, 6.2, −1.5]	3.9	1.0
Trial 2 (*left hip*)				
Gold standard	[−0.8, −7.9, −1.0]	[−2.1, −0.7, −1.9]	0	0
BGS	[−0.3, −9.4, −2.0]	[0.0, −0.2, −2.3]	1.8	2.2
PCR	[0.4, −8.4, −1.6]	[−2.7, −0.5, −0.3]	1.4	1.8

"Gold Standard" uses fiducials placed in the specimen; "BGS" is computed intraoperatively using the system; "PCR" is the postoperative contour registration. Positive rotations about X rotate the fragment backwards about a medial-lateral axis; positive rotations about Y indicate lateral rotation; positive rotations about Z correspond to retroversion

Table 2 Difference of CT-based and X-ray image projection angles automatically computed for varying approaches on instrumented cadavers compared with the gold standard, where fiducials are placed in the specimen

	CT reformats				X-ray projection images	
	F-CE	F-AC	S-AC	AcAV	CE	AC
Trial 1 (*left hip*)						
BGS	−0.5	0.4	0.6	2.2	−0.7	0.6
PCR	0.8	−0.8	1.5	3.7	2.4	−2.1
Postop	4.9	−1.0	−8.1	−0.3	−2.3	3.6
Trial 2 (*left hip*)						
BGS	1.6	−1.9	0.2	1.2	1.8	−1.7
PCR	0.5	−1.0	0.6	0.9	0.8	−0.8
Postop	−4.9	0.7	−2.1	−0.2	−2.6	−1.3

"BGS" is computed intraoperatively using the system; "PCR" is the postoperative contour registration. "Postop" uses the acetabular lunate segmented directly from the postoperative CT scan. All measurements are in degrees

ter matched the PCR measurements than the postoperative measurements (Table 3). The difference between BGS and PCR for the F-CE angle was $-0.2° \pm 5.3°$, compared to $-7.6° \pm 7.5°$ for the difference between BGS and direct postoperative measurement. For the F-AC angle, the results showed $0.8° \pm 4.3°$ as the difference between BGS and PCR compared to $2.8° \pm 4.4°$ for the difference between BGS and direct postoperative measurement. Considering the difference between intra- or postoperative anatomical angle measurements (i.e., BGS, PCR, or direct postoperative) and the preoperative anatomical angle measurements, a one-way ANOVA identified a significant difference between the three measurements ($p = 0.003$). A Tukey honestly significant difference test indicated that the mean of the postoperative group was significantly different from that of BGS and PCR. The improvements (e.g., confidence points) added to the system during these tests did not adversely affect the outcomes, and the surgeons reported increased utility of the system following these changes.

The following list of modifications occurred throughout the testing procedure. This list is not exhaustive; however, it reflects incremental system enhancements and verification with cadaveric specimen.

Confidence points The addition of four confidence points (Fig. 5) on the fixed pelvis region helped minimize errors and recover from accidental shifts of the reference body. This was performed after noticing unintended movement of the reference geometry, and was implemented in surgeries 10 and later.

Reference fixation Affixing the reference geometry ipsilaterally may result in more accurate results (it is closer to the osteotomy) and eliminate the need for a contralateral incision. However, this may result in increased occlusion or impede the surgical flow. The seven final surgeries were performed with an ipsilateral attachment.

Femoral range of motion Femoral range of motion (including hip flexion/extension, adduction/abduction, internal/external rotation, and circumduction) can be captured and compared before and after fragment repositioning. The range of motion was captured by affixing a reference geometry to the leg and measuring the position with respect to the pelvis. This change was included in the final seven surgeries.

Radiographic projections The inclusion of intraoperative visualization of radiographic projections based on the collected data improves information presented to the surgeon. The digitally reconstructed radiographs (DRR) are created by projecting tetrahedra of the pelvis model onto a simulated 2D radiographic plane [32,33]. Moreover, if the pelvis is split into the rigid and fragmented portion, the DRR will display the repositioned acetabulum.

Table 3 CT-based and X-ray image projection angles automatically computed for varying approaches on non-instrumented, intact cadavers with clinically relevant exposures

Trial number	1	2	3	4	5	6	7	8	9	10	11	12	13	14	15	16	17
F-CE																	
Preop	35.6	36.2	38.0	44.5	34.5	38.0	43.2	42.5	30.1	40.5	35.1	34.7	37.6	32.1	37.5	40.2	39.6
BGS	49.5	16.3	58.7	52.0	52.5	51.6	54.3	39.0	32.5	46.1	37.5	37.5	40.6	51.2	44.2	38.8	43.3
PCR	34.9	20.9	64.0	60.7	50.8	50.9	58.8	42.1	30.0	45.7	36.8	36.3	45.8	45.6	41.9	40.8	43.3
Postop	43.3	38.5	69.1	63.1	62.9	64.4	57.7	61.2	28.8	53.0	40.0	42.7	46.5	56.3	47.5	45.0	53.9
F-AC																	
Preop	5.6	6.8	−5.8	−7.9	0.6	−6.4	0.6	−4.2	15.4	−3.1	12.0	14.9	2.4	7.1	−5.6	−0.9	−2.1
BGS	−2.6	30.6	−27.1	−15.8	−11.7	−15.5	−12.2	−0.2	13.1	−6.3	10.0	11.0	−7.2	−5.3	−6.1	0.0	−5.3
PCR	8.2	25.0	−32.1	−22.7	−10.9	−13.3	−15.5	−1.7	15.3	−5.6	10.8	12.0	−9.7	−6.1	−12.5	−1.7	−3.3
Postop	2.4	19.6	−32.3	−21.1	−7.5	–	−15.4	−6.2	12.5	−7.9	7.9	10.7	−10.9	−11.5	−15.7	1.3	−5.9
S-AC																	
Preop	−35.1	−39.2	−28.9	−33.3	−34.1	−32.0	−38.0	−40.4	−32.5	−34.5	−38.8	−35.4	−38.0	−33.4	0.0	0.0	−29.9
BGS	−47.7	−65.4	–	−36.4	−40.5	−36.6	−44.7	−54.3	−33.4	−37.7	−42.4	−37.9	−52.5	−50.5	0.0	0.0	−32.2
PCR	−40.8	−52.0	–	−37.3	−39.1	−37.8	−46.2	−49.5	−33.2	−38.3	−41.7	−38.1	−47.7	−48.3	0.0	0.0	−31.2
Postop	−43.8	−78.4	−36.2	−35.6	−44.1	−60.7	−44.3	−69.5	−33.9	−35.8	−42.0	−39.4	−45.3	−52.6	0.0	0.0	−38.4
AcetAv																	
Preop	15.1	13.8	21.6	16.9	23.0	21.1	9.3	9.7	18.7	22.8	7.9	13.0	12.2	10.9	15.0	20.8	19.7
BGS	−17.8	−20.7	18.4	15.3	17.8	18.5	−5.5	−25.4	21.0	18.8	0.9	6.0	−18.6	−31.2	−11.2	21.6	17.6
PCR	4.3	−13.3	24.4	9.2	20.7	14.7	−16.4	−16.6	16.8	18.2	1.3	5.7	−9.2	−15.6	4.4	22.9	13.5
Postop	0.8	−14.6	25.9	10.2	18.8	16.3	−22.9	−17.7	16.6	17.3	1.7	4.7	−7.1	−19.6	0.8	21.4	14.5
CE																	
Preop	35.6	38.4	43.3	46.3	34.5	38.5	46.2	42.7	44.3	45.6	35.2	34.6	40.2	33.6	37.6	41.0	39.2
BGS	55.0	51.8	63.4	54.0	53.5	52.1	60.3	62.0	51.4	46.8	39.7	37.4	57.2	55.5	46.7	38.7	43.1
PCR	38.5	51.5	67.4	62.1	51.4	51.4	69.8	55.9	42.5	45.8	39.9	36.3	55.7	49.9	42.3	41.0	43.2
Postop	44.8	66.4	71.6	67.7	63.3	65.4	65.5	60.2	29.1	53.6	40.4	42.3	56.9	58.6	47.3	45.5	54.1
AC																	
Preop	5.7	3.7	−9.3	−8.7	−0.8	−7.4	−1.6	−4.0	0.1	−10.3	11.1	13.0	−1.6	6.0	−7.7	−2.5	−1.7
BGS	−9.1	5.5	−29.2	−16.9	−17.2	−19.1	−16.3	−17.9	−4.4	−10.1	7.3	9.5	−18.1	−11.6	−16.3	−1.4	−5.3
PCR	3.9	2.0	−34.5	−23.6	−15.5	−18.2	−21.7	−14.3	0.5	−8.0	6.9	10.7	−15.4	−9.3	−13.0	−3.4	−4.5
Postop	0.1	−3.2	−33.4	−24.5	−11.4	−20.9	−19.1	−5.4	11.6	−8.6	7.5	10.4	−19.2	−14.6	−15.4	−2.2	−6.0

"Preop" are the preoperative angles; "BGS" are the angles computed intraoperatively using the system; "PCR" are the angles computed using the postoperative contour registration; "Postop" computes the angles from the acetabular lunate segmented directly from the postoperative CT scan. (−) values represent those conditions where the requisite anatomical features were not visible on the CT reformat. All measurements are in degrees

Discussion

This paper presents a surgical navigation system that combines a patient-specific, real-time biomechanical model of the hip joint with automated algorithms that compute simulated radiological joint repositioning angles. The novel aspect of this system is the ability to link a subject-specific biomechanical model to a navigation system such that the surgeon can use the feedback information to take corrective actions during surgery to achieve the ideal joint repositioning rather than waiting for a postoperative definitive assessment. The accuracy study described presently evaluated the system in two instrumented cadaveric tests. Additional intact cadaver studies evaluated system refinements and procedural techniques.

Evaluation of the two instrumented cadaver studies shows high system accuracy cadaver studies (1.4 and 1.8 mm, and 1.0° and 2.2°). This end-to-end system accuracy includes errors introduced from a number of sources including: the segmentation of the pelvis from the CT image volume, navigation system, digitization of the bone burrs, co-registration of the preoperative and postoperative CT scans, and picking fiducial (screw) locations from the CT scans. As expected, the change in CE (F-CE) and AC (F-AC) angles closely corresponded to the Euler decomposition of rotations about the y axis. The small difference between the ICP and UKF reg-

istration indicate that the faster ICP algorithm is appropriate for this surgery.

The seventeen additional cadaver studies demonstrated system robustness and procedural refinement. Moreover, this set of tests verified that the BGS measures anatomical angles accurately compared to the PCR results. The discrepancy from the direct postoperative evaluation potentially comes from changes in the postoperative segmentation of the acetabular surface—since the anatomical angles are based on the geometry of the acetabulum, a change in both position (due to the surgery) and geometry (due to the postoperative segmentation) will have increased error compared to only the change in position (i.e., the angles computed through the PCR routine). Considering only anatomical angles on CT reformats, there is no significant difference between the three groups ($p = 0.84$); however, comparing only the anatomical angles measured on X-ray projection images identifies the direct postoperative evaluation as significantly different from the BGS and PCR approaches ($p < 0.001$).

Incremental changes were made to the protocol throughout the testing process based on feedback from the operating surgeon and improvements in software. These changes increased efficiency, accuracy, communication with the surgeon, and workflow. Non-navigated surgical procedures were interleaved within the navigation process to minimize downtime while the navigation system is computing, improving efficiency. Occasional difficulties in placing the fragment bone burrs resulted in a protocol change where the most superior cut was performed before creating the bone burrs to provide a clear distinction between fragment and fixed pelvis. The inclusion of confidence points on the ilium allowed the system to recover from errors due to accidental movement of the reference geometry. Moreover, this approach enabled the placement of the reference geometry on the ipsilateral side since it can be detached during operation so as not to interfere with the surgeon, and reattached during measurements with the BGS system.

Hip impingement is a common concern in treatment of dysplasia due to overcorrection [2,6]. The inclusion of the femur range of motion module will help the surgeon identify and compare pre- and intraoperative motion capabilities. This assessment will provide quantitative information on the risk of impingement postoperatively. As the hips used in this study were normal, the testing of the range of motion was more a demonstration of capabilities; future clinical studies should report on the range of motion assessment with regard to postoperative impingement. Moreover, one can consider adding the simulation of the hip range of motion to the preoperative biomechanical planning module of the BGS to help avoid impingement in the planned repositioning of the acetabulum.

As described, the BGS reports specific biomechanical and geometric characterization metrics to the surgeon. A collaborating surgeon (JL) who has performed over 350 PAO cases helped to define these specific metrics based on his experience. However, other surgeons may rely on different metrics related to their specific approach (e.g., consistency of the Shenton line or predicted impingement). Tailoring the BGS to a specific surgeon through the inclusion of these metrics would make the BGS more accessible to other surgeons and help improve the overall system.

Unlike the procedure described for the BGS, conventional PAO surgery does not include a CT scan of the full pelvic region. Conventional procedure is to obtain standing anteroposterior and lateral radiographs, potentially with the addition of a CT of the joint region. As such, the BGS would expose the young, female patient population to additional radiation. However, an alternative approach not used in this study combines statistical atlases with 2D/3D registration to estimate the full pelvic geometry from a CT scan of only the joint region [34]. This approach has shown potential in accurately estimating the pelvic geometry and will be used in the future studies on the system.

The following are some of the limitations of the present study. First, the validation experiments were performed on non-dysplastic cadavers (normal hips), whereas the intended population benefitting from the BGS would be individuals with dysplasia. Available cadaver specimens were elderly, with weaker and more brittle bone than young patients who undergo PAO. Performing arbitrary acetabular repositioning on normal hips does not have clinical relevance—it may, among other things, increase the risk of impingement as evidenced by the resultant high center edge angles [35]. However, the primary intent of this validation study was to quantify system and navigation error. As such the osteotomy was performed in the traditional sense as if the hip were dysplastic. No attempt was made to simulate dysplasia in these cadavers. The system tracking error analysis is unaffected by the presence or absence of dysplasia, and as such we believe that our results convey to either population. Secondly, the system accuracy studies involved disarticulating the cadaveric hip joints to instrument the cadaver hips with fiducials in the pelvis and acetabulum. This results in unrealistic surgical exposure and mobility of the acetabulum. While this affects the ultimate location of the acetabulum, our analysis compares the relative predicted versus actual location of the fragment, rather than the absolute location. Finally, the scope of this study is limited to the ability to navigate the acetabular fragment using the BGS. Previous studies assessed the biomechanical [9,10] and angle estimation [15] modules, while planned future studies will assess the BGS in surgical practice.

In conclusion, this system represents the first time that navigation, biomechanics, and geometric characterization of the acetabulum have been combined to provide real-time feedback during PAO. Recent studies suggest the utility

of this intraoperative feedback in improving survivorship of PAO [5,6]. The cadaveric studies showed the estimated accuracy with the BGS appears acceptable for future surgical applications. This study also uncovered and addressed improvements to the BGS, improving feasibility for future clinical studies.

Acknowledgments The authors thank Dr. Stephen Belkoff for the use of his cadaver lab, and Mr. Demetries Boston for his assistance during cadaveric testing. This work was funded through Grant R01EB006839-01 National Institute of Biomedical Imaging and Bioengineering (NIBIB) of the National Institutes of Health (NIH), and internal funds from the Johns Hopkins University.

Conflict of interest The authors declare that they have no conflict of interest.

Ethical standard All cadaveric specimens used in this study were acquired through the Maryland State Anatomy Board under IRB exemption approval through Johns Hopkins Medical Institutions. The co-authors have completed Hyman Subject Research (HSR) and Research Ethics (REWards) or equivalent training.

References

1. Ganz R, Klaue K, Vinh TS, Mast JW (1988) A new periacetabular osteotomy for the treatment of hip dysplasias. Technique and preliminary results. Clin Orthop Relat Res 232:26–36
2. Hussell JG, Rodriguez JA, Ganz R (1999) Technical complications of the Bernese periacetabular osteotomy. Clin Orthop Relat Res 363: 81–92
3. Cooperman DR, Wallensten R, Stulberg SD (1983) Acetabular dysplasia in the adult. Clin Orthop Relat Res 175:79–85
4. Troelsen A (2009) Surgical advances in periacetabular osteotomy for treatment of hip dysplasia in adults. Acta Orthop Suppl 80:1–33
5. Albers CE, Steppacher SD, Ganz R, Tannast M, Siebenrock KA (2013) Impingement adversely affects 10-year survivorship after periacetabular osteotomy for DDH. Clin Orthop Relat Res 471:1602–1614
6. Troelsen A, Elmengaard B, Søballe K (2009) Medium-term outcome of periacetabular osteotomy and predictors of conversion to total hip replacement. J Bone Joint Surg Am 91:2169–2179
7. Langlotz F, Bachler R, Berlemann U, Nolte LP, Ganz R (1998) Computer assistance for pelvic osteotomies. Clin Orthop Relat Res 354: 92–102
8. Langlotz F, Stucki M, Bachler R, Scheer C, Ganz R, Berlemann U et al (1997) The first twelve cases of computer assisted periacetabular osteotomy. Comput Aided Surg 2:317–326
9. Armand M, Lepistö J, Tallroth K, Elias J, Chao E (2005) Outcome of periacetabular osteotomy: joint contact pressure calculation using standing AP radiographs, 12 patients followed for average 2 years. Acta Orthop 76:303–313
10. Armiger RS, Armand M, Tallroth K, Lepistö J, Mears SC (2009) Three-dimensional mechanical evaluation of joint contact pressure in 12 periacetabular osteotomy patients with 10-year follow-up. Acta Orthop 80:155–161
11. Hipp JA, Sugano N, Millis MB, Murphy SB (1999) Planning acetabular redirection osteotomies based on joint contact pressures. Clin Orthop Relat Res 364: 134–143
12. Tsumura H, Kaku N, Ikeda S, Torisu T (2005) A computer simulation of rotational acetabular osteotomy for dysplastic hip joint: does the optimal transposition of the acetabular fragment exist? J Orthop Sci 10:145–151
13. Armiger RS (2006) Development of a surgical guidance system for real-time biomechanical feedback during periacetabular osteotomy (Master's thesis). Master's thesis, Johns Hopkins University, Baltimore, MD
14. Lepistö J, Armand M, Armiger RS (2008) Periacetabular osteotomy in adult hip dysplasia—developing a computer aided real-time biomechanical guiding system (BGS). Suom Ortoped Traumatol 31:186–190
15. Armiger RS, Armand M, Lepistö J, Minhas D, Tallroth K, Mears SC et al (2007) Evaluation of a computerized measurement technique for joint alignment before and during periacetabular osteotomy. Comput Aided Surg 12:215–224
16. An KN, Himeno S, Tsumura H, Kawai T, Chao EY (1990) Pressure distribution on articular surfaces: application to joint stability evaluation. J Biomech 23:1013–1020
17. Genda E, Konishi N, Hasegawa Y, Miura T (1995) A computer simulation study of normal and abnormal hip joint contact pressure. Arch Orthop Trauma Surg 114:202–206
18. Volokh K, Chao E, Armand M (2007) On foundations of discrete element analysis of contact in diarthrodial joints. Mol Cell Biomech 4:67–73
19. Armand M, Merkle A, Sukal T, Kleinberger M (2002) Experimental evaluation of a model of contact pressure distribution in the hip joint. In: Proceedings of world congress on biomechanics, Calgary, Alberta
20. Elias J, Wilson D, Adamson R, Cosgarea A (2004) Evaluation of a computational model used to predict the patellofemoral contact pressure distribution. J Biomech 37:295–302
21. Michaeli DA, Murphy SB, Hipp JA (1997) Comparison of predicted and measured contact pressures in normal and dysplastic hips. Med Eng Phys 19:180–186
22. Schuind F, Cooney W, Linscheid R, An K, Chao E (1995) Force and pressure transmission through the normal wrist. J Biomech 28:587–601
23. Murphy SB, Kijewski PK, Millis MB, Harless A (1990) Acetabular dysplasia in the adolescent and young adult. Clin Orthop Relat Res 214–223
24. Tallroth K (2006) Developmental dysplasia of the Hip 2: adult. In: Davies AM, Johnson KJ, Whitehouse RW (eds) Imaging of the hip and bony pelvis: techniques and applications, medical radiology. Springer, Berlin, pp 125–140
25. Lepistö J, Tallroth K, Alho A (1998) Three-dimensional measures of acetabulum in periacetabular osteotomy. In: Orthopaedic research society 44th annual meeting
26. Anda S, Terjesen T, Kvistad KA (1991) Computed tomography measurements of the acetabulum in adult dysplastic hips: which level is appropriate? Skeletal Radiol 20:267–271
27. Anda S, Terjesen T, Kvistad KA, Svenningsen S (1991) Acetabular angles and femoral anteversion in dysplastic hips in adults: CT investigation. J Comput Assist Tomogr 15:115–120
28. Wiberg G (1939) Studies on dysplastic acetabula and congenital subluxation of the hip joint with special reference to the complications of osteoarthritis. Acta Chir Scand 83:53–68
29. Tönnis D (1987) Congenital dysplasia and dislocation of the hip in children and adults. Springer, Berlin
30. Besl PJ, McKay ND (1992) A method for registration of 3-d shapes. IEEE Trans Pattern Anal Mach Intell 14:239–256
31. Moghari MH, Abolmaesumi P (2005) A novel incremental technique for ultrasound to CT bone surface registration using unscented Kalman filtering. Med Image Comput Comput Assist Interv 8:197–204
32. Sadowsky O, Cohen JD, Taylor RH (2005) Rendering tetrahedral meshes with higher-order attenuation functions for digitial radiograph reconstruction. In: Visualization conference, IEEE p 39

33. Sadowsky O, Cohen JD, Taylor RH (2006) Projected tetrahedra revisited: a barycentric formulation applied to digitial radiograph reocnsturation using higher-order attenuation functions. IEEE Trans Vis Comput Graph 12:461–473
34. Chintalapani G, Murphy R, Armiger R, Lepisto J, Otake Y, Sugano N, et al (2010) Statistical atlas based extrapolation of CT data. In: SPIE medical imaging, international society for optics and photonics, p 762539
35. Kutty S, Schneider P, Faris P, Kiefer G, Firzzel B, Park R, Powell JN (2012) Reliability and predicatability of the centre-edge angle in the assessment of pincer femoroacetabular impingement. Int Orthop 36(3):505–510